Journal of Thermal Analysis and Calorimetry, Vol. 56 (1999) 1423-1433

INFLUENCE OF OPERATING CONDITIONS ON $BaSO_4$ CRYSTAL SIZE AND MORPHOLOGY IN A CONTINUOUS COUETTE PRECIPITATOR

*S. Pagliolico, D. Marchisio and A. A. Barresi**

Dipartimento di Scienza dei Materiali ed Ingegneria Chimica – Politecnico di Torino, Corso Duca degli Abruzzi, 24 – 10129 Torino, Italy

Abstract

Precipitation of a sparingly soluble salt in the annular gap of a continuous Couette reactor with two unpremixed feeds has been experimentally investigated. Barium chloride and sodium sulphate in stoichiometric ratio are fed at different flow rate in the lower part of the reactor; different feeding modes have been considered. The dependence of precipitation yield, mean crystal size and particle size distribution on rotation speed, axial flow rate and initial supersaturation ratio has been studied. Depending on the operating conditions crystals with different morphologies have been obtained, varying from dentritic tabular crystals to complex pyramidal ones and from single crystals to aggregates.

Keywords: $BaSO_4$, Couette reactor, morphology, precipitation

Introduction

The control of the morphology and characteristics of the powders produced by precipitation, that is reactive crystallisation of sparingly soluble salts, is of relevant interest in the modern chemical industry; silver halide crystals for photographic applications, just to make an example, are prepared by this way.

Precipitation is a three steps process: reaction in the liquid phase (usually very fast or almost instantaneous), nucleation and crystal growth; as at least the first two steps are very fast, the process is 'mixing sensitive', that is its rate is not determined by kinetics alone but there is a strong influence of the turbulent transport phenomena and, more generally, of the hydrodynamics of the apparatus. Micromixing controls the generation of supersaturation, bringing the unpremixed reactants into contact, and its redistribution, by dilution; mesomixing (which describes the interaction of the plume of fresh feed with its surrounding and the inertial-convective disintegration of the large eddies) and macromixing determine the environment in which micromixing takes place, influencing indirectly the distribution of supersaturation [1, 2].

* Author for correspondence: e-mail: pagliol@polchil.polito.it; barresi@athena.polito.it
fax: +39-011-5644699

1418–2874/99/ $ 5.00

Akadémiai Kiadó, Budapest
Kluwer Academic Publishers, Dordrecht

As nucleation and growth are in competition, and are influenced by the local value of the supersaturation, both the crystal size distribution and the morphology of the crystals are influenced by the turbulent mixing sequence and thus by the operating conditions.

The precipitation of barium sulphate is generally adopted as test reaction, because the product has a rich morphology, the solubility is extremely low, the reactants are not expensive and the nucleation and growth kinetics are relatively well known; in fact, many studies have been carried on this reaction, because it has a high economic relevance, being responsible of scaling in off shore drilling [3–11].

The dependence of crystal morphology and size on the fluid dynamics of mixing has been evidenced long time ago [4], but only in recent years the effects of feeding mode (i.e. premixed or unpremixed, single or double jet, feed tube diameter and position) and the influence of the operative parameters (e.g. reactants flow rate, volumetric ratio, velocity and concentration, stirrer speed and power input) in industrial apparatus have been deeply investigated. Jet mixing reactor and mixing tee [12–15], stirred tank reactor operated in semibatch [7, 12, 16–18] and in continuous mode [19–22] have been considered, evidencing that the variation of an operative parameter can produce opposite effects in different apparatus.

In this work the precipitation of barium sulphate in a continuous Couette reactor operating in the region of turbulent vortex flow and fully turbulent flow will be investigated.

The properties of the Couette reactor are particularly interesting for controlled precipitation processes: its hydrodynamics is much more simple than that of a stirred vessel, the average shear rate and power dissipation rate are relatively uniform in the axial direction and there are no blade type mixers, which can cause the breakage of the crystals. The radial and circumferential mixing is always very good, and increasing the rotation speed of the internal cylinder the average energy dissipation rate and micromixing increase significantly; the axial dispersion also increases with the rotation speed, and is thus possible to change the macromixing characteristics of the device passing from that close to a plug flow to that of a well mixed system. The hydrodynamics of the continuous Couette cell in turbulent regime has been investigated in a previous work [23] that has evidenced how this type of apparatus can be employed successfully for precipitation processes.

Experimental set-up

The $BaSO_4$ precipitation reaction in water solution has been tested, using unpremixed feeds of $BaCl_2$ and Na_2SO_4; the solutions were prepared from reagent grade anhydrous salts (supplied by Fluka) and distilled water and are fed to the bottom of the Couette cell.

The Couette reactor is equipped with a jacket and a thermostatic system to control the temperature (25°C). The internal cylinder (125 outer diameter and 475 mm long) is made of PVC, while the external one (175 internal diameter and 500 mm long) is in Plexiglas; the annular gap/inner radius ratio (d/r_1) is 0.4, while the aspect ratio (H/d) is 19. Further details of the experimental set up can be found in a previous work [23].

The two reactants were fed in stoichiometric ratio, but at different concentration: in all the runs the barium solution was at a concentration ten times higher than the sulphate solution, and therefore the flow rate was only 1/10; three different flow rates were investigated, 150–15, 250–25 and 350–35 l h^{-1}, corresponding to an axial Reynolds number ($Re_z=<w>d/\nu$) varying from 100 to 240. The rotation velocity of the inner cylinder was varied in the range 200–900 rpm ($Re=r_1\Omega_1 d/\nu$=35.000–170.000) by means of a variable speed DC motor.

The sulphate solution was fed through a 25 mm nozzle in the bottom of the Couette cell, while several different feeding modes were considered for the barium chloride solution: in mode A a 25 mm or a 2 mm nozzle in the bottom of the cell is used (the two nozzles are diametrically opposed, with an inter-axes distance of 90 mm); in mode B a tube with a tangential exit in the middle of the annular gap 40 mm above the bottom of the inner cylinder has been adopted: three feed tubes with different internal diameter (a=2, 3 and 4 mm respectively) have been tested.

The influence of the initial supersaturation ratio $S=[Ba^{2+}][SO_4^{2-}]/K_{ps}$ was investigated in the range from 10^5 to 10^6 (corresponding to a calculated concentration of each of the two reactants varying from to $3.4\cdot10^{-4}$ to $1.1\cdot10^{-2}$ M), while the effect of the other operating parameters was studied mainly at a nominal initial saturation ratio (calculated supposing perfect mixing of the reactants) of 10^4.

The concentration of the crystals was measured by a gravimetric technique, filtering the suspension over a 1 μm filter; the residual supersaturation in the outlet stream was measured using the conductimetric technique proposed by Gunn and Murthy [3]. This allowed to verify the material balance, that resulted satisfied with an error of 1–5% (a comparison of the values of solid concentration measured by filtration and calculated from residual ion concentration in the liquid is shown in Fig. 8); in a few runs the barium residual concentration was measured by atomic absorption. The crystal size distribution was detected by a Malvern particle sizer 3600 D, while the crystal morphology was observed with a scanning electron microscope.

Results and discussion

Dependence of crystal morphology on operative conditions

The prevailing morphology is strongly affected by the supersaturation level, while the other operative parameters have a weak effect. At high supersaturation dendritic crystals are formed as a consequence of the bulk diffusion control; a similar habitus was observed previously by other authors [3, 4, 15, 21]. Figure 1 shows an example.

At lower supersaturation rounded tabular crystals with a characteristic pyramidal overgrowth are obtained (Fig. 2); in fact, at these conditions surface nucleation becomes important [4, 7]. At $S=10^6$ the pyramidal growth is virtually absent when a large (25 mm) nozzle is used (Fig. 1) or is very little developed when a small diameter feed tube is used. It is also possible that adsorbed sodium ions on the surface of the crystals may serve as active centres for surface nucleation during the crystalisation process [4].

The operative conditions seem to have an effect on the sharpness of the crystals; it can be noted comparing Figs 3a, b and 4 that with smaller feed tube diameter and

Fig. 1 Dendritic crystals obtained at high initial supersaturation ratio ($S=10^6$) with feed from a large nozzle in the bottom (mode A, 25 mm); Q=250–25 l h^{-1}, N=520 rpm. d_{43}=14.6 µm

Fig. 2 Tabular crystals with pyramidal growth and rose aggregates obtained at lower supersaturation ratio ($S=10^4$). Mode A, 25 mm; Q=150–15 l h^{-1}; N=600 rpm. d_{43}=5.1 µm

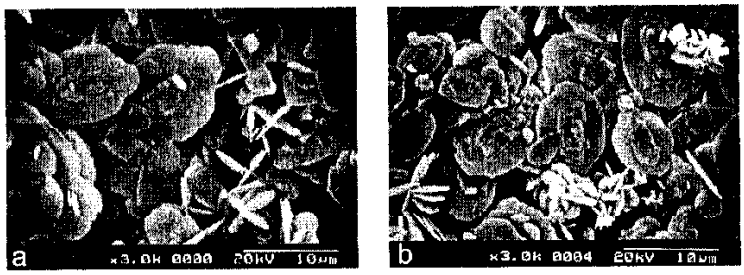

Fig. 3 Effect of the rotation speed on morphology: tabular crystals with pyramidal growth prevail, but smaller twin crystals form at lower speed (left photo) and rose aggregates form at higher speed (right photo). Feed mode B (a=3 mm); $S=10^4$; Q=385 l h^{-1}. a) N=200 rpm, d_{43}=6.6 µm. b) N=900 rpm, d_{43}=6.1 µm

higher rotation velocity the base plate appears more regular; this can be related to the different influence of mesomixing, that changes the history of supersaturation.

Other morphologies have been observed in the experiments carried out at lower suspersaturation, even if they account for a minor fraction of the crystals formed: following the classification proposed by Bernard-Michel *et al.* [24], they can be de-

scribed as pyramidal flowers and roses; Figs 4 and 5 show a detail. Pyramidal flowers are single or complex twins, formed with pyramidal crystals: their size very rarely is equal to that of the simple crystals, generally they are smaller. Multiple twinned crystals were obtained by Baldyga *et al.* [7] in semi-batch operation feeding both reactants in the high energy dissipation rate impeller region; in this work it was observed that increasing the rotation speed it was more probable the formation of regular flowers, instead of single twins, while at high rotation speed are more common small irregular aggregates (roses), similar to the 'ordered aggregates' observed by Baldyga *et al.* [17] (Figs 3a, b).

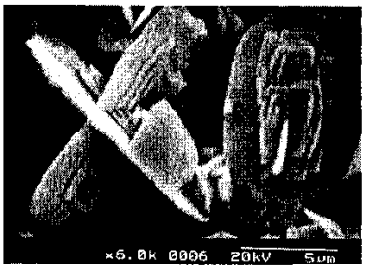

Fig. 4 Detail of a twin crystal, with simple tabular crystal and rose. Mode A (a=2 mm): Q=165 l h^{-1}; N=800 rpm; S=10^4

Fig. 5 Detail of rose aggregates. Mode A (a=3 mm); Q=385 l h^{-1}; N=900 rpm; S=10^4

It can be pointed out that in this work the rose aggregates have been produced increasing the rotation speed and thus the mixing intensity; Fitchett and Tarbell [21] observed that at high feed concentration (0.15 M) the particles no longer have a base plate but rather consist of smooth-edged platelets that are joined by edge contact. The platelets retain the predominantly orthogonal orientation displayed at lower concentrations, but there is no dominant base plate.

In no case were regular single crystals observed; these are typical of very low supersaturation values [3, 4, 6, 17, 25].

As the crystals are thin platelets (the thickness is variable between 0.5 and 2 μm), and thus far from spherical, for some selected runs the SEM photographs have been

analysed in order to evaluate the average particle size and to compare it with the measured one: the value given by the instrument (and reported in the following figures) is intermediate between the values of the length and width of the tabular crystals, but generally closer to the second one. The measured particle diameters are given for Figs 1–3 to allow a comparison.

Table 1 Surface and volume shape factors for the different crystal morphologies

Morphology	k_a	k_v	Φ_v
Tabular (dendritic)	1.1	0.05	0.46
Tabular (with pyramidal growth)	1.6	0.05–0.07	0.46–0.51
Simple twin	2.4	0.07–0.09	0.51–0.56
Rose	5.8	0.3–0.4	0.83–0.91

The surface and volume shape factors for the different morphologies have also been evaluated and are shown in Table 1. There is a large variation in the values reported in the literature, but this is partly due to differences in definition and uncertainty in the choice of the characteristic crystal dimension [3, 7, 14, 20, 21].

The surface and volume shape factors are defined respectively as

$$A_p = k_a L^2 \tag{1}$$

$$V_p = k_v L^3 = \frac{\pi d_s^3}{6} \tag{2}$$

As characteristic size the main dimension has been chosen for the dendritic and pyramidal crystals (the width to length ratio varies between 0.5 and 0.7); it is related to the diameter of sphere of the same volume, d_s, through the sphericity factor, Φ_v:

$$L = \left(\frac{\pi}{6k_v}\right)^{1/3} d_s = \frac{d_s}{\Phi_v} \tag{3}$$

For well formed and pyramidal tabular crystals values of k_a in the range 1.5÷2 have been reported, similar to those measured in this work. Higher values have been obtained, as expected, for twins and aggregates; in this case the diameter of the enclosing sphere has been chosen as characteristic dimension.

Dependence of crystal size on operative conditions

The initial supersaturation is the parameter that has the strongest effect on the final crystal size, but the dependence of the latter on S is also significantly influenced by the feed mode adopted. Figure 6 shows that larger variations are observed at higher flow rate, while the diameter of the feed tube is also important: this can be explained considering that the size of the feeding port and the flow rate determine the size of the segregated reacting plume and its disintegration time, causing a differ-

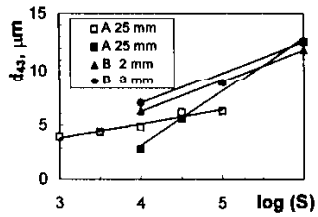

Fig. 6 Dependence of crystal size on supersaturation ratio for different $BaCl_2$ feeding modes. Open symbols, Q=150–15 l h^{-1}; filled symbols, Q=250–25 l h^{-1}

ence in the value of the local supersaturation generated in each fluid lump and in its variation with time during the lump life. An example of the dependence of the crystal size distribution on the supersaturation ratio is shown in Fig. 7; it can be noted that the distribution becomes broader, but the variation coefficient, defined as the ratio of the standard deviation and the average size, remains almost constant.

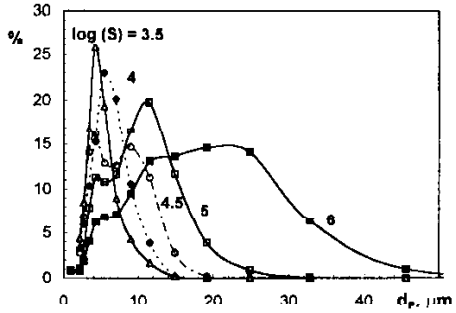

Fig. 7 Dependence of crystal size distribution on initial supersaturation ratio. N=520 rpm; Q=275 l h^{-1}; feed mode A (a=25 mm)

It must be remembered that the value of supersaturation determines the growth controlling mechanism (bulk diffusion or surface reaction), as evidenced by the different morphologies [26], and the number of crystals formed, as a consequence of the strong non-linear dependence of nucleation rate on supersaturation; higher values of supersaturation cause higher nucleation rates and finally a bigger number of smaller crystals. Figure 8 shows that in the conditions tested the yield in crystals (and the solid concentration in the suspension) increases with the initial supersaturation, but the supersaturation at the outlet is low and practically constant; no significant variations have been observed with rotation speed and residence time (for the flow rates investigated it is 144, 86 and 61 s), indicating that the precipitation process is virtually complete. From the analysis of the experimental data it can be concluded that even if at higher supersaturation bigger crystals are obtained, the increase in the crystal volume is significantly smaller than the increase in the reactant concentration, evidencing that a larger number of crystals is formed: it can be esti-

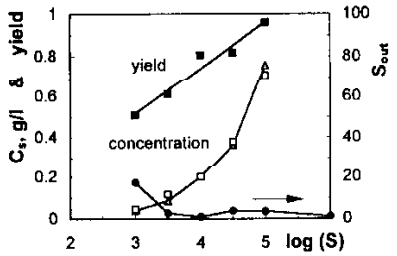

Fig. 8 Supersaturation ratio at the outlet (•) and crystal yield (■) as a function of the inlet supersaturation ratio (feed mode A, a=25 mm; Q=275 l h^{-1}; N=520 rpm). The values of the crystal concentration in suspension measured by conductimetry (□) and by filtration (△) are also shown

mated that a fivefold increase in the crystal number occurs for a variation of the supersaturation ratio from 10^3 to 10^5.

Rotation speed and flow rate have a weaker influence on the crystal size, but the dependence on this parameters is quite complex. Figure 9 shows that a maximum can be obtained varying the rotation speed: this is probably the result of a competition between nucleation and growth, but considering the large variation in the energy input (the estimated power input varies from 0.1 to 7 kW kg^{-1}) and also the change in the gross hydrodynamics [23], it can be considered a minor effect. The size and position of the feed port seem to have the greatest effect: with the 25 mm nozzle in the bottom of the cell (mode A), smaller crystals are obtained, and with this configuration there is a large sensitivity to the axial velocity. The curves at different flow rate are much closer to each other when the small diameter tube is used, and there is also a very small difference between the performance of the 2 mm nozzle on the bottom (mode A) and the 2 mm tube (mode B).

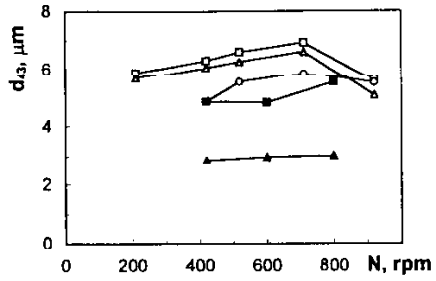

Fig. 9 Dependence of crystal diameter on rotation speed and total flow rate; S=10^4. □■, Q=165 l h^{-1}; △▲, Q=275 l h^{-1}; ○, Q=385 l h^{-1}. Open symbols: 2 mm diameter feed tube (mode B); filled symbols: 25 mm bottom feed (mode A)

The dependence of particle size on flow rate and feed tube diameter (mode B) is shown in Fig. 10: the differences in the average crystal size obtained using feed tubes of different diameter are very small at low rotation speed, but become more significant at higher Reynolds; to explain the complex dependence on flow rate and

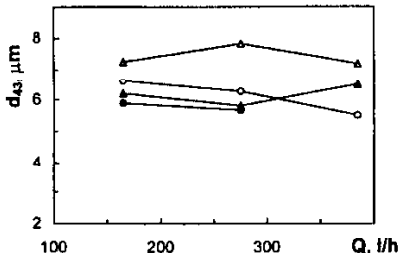

Fig. 10 Effect of total flow rate and tube feed diameter (mode B) on the crystal size; $S=10^4$. ○ ●, a=2 mm; △ ▲, a=4 mm. Filled symbols, N=200 rpm; open symbols, N=500 rpm

the influence of the rotation speed, the different contributions of micro- and mesomixing depending on the value of these variables must be considered. The characteristic time for micromixing decreases at higher rotation speed, because the turbulent energy dissipation rate increases; the characteristic time for turbulent dispersion of the species A can be defined as:

$$\tau_d = Q_A/\bar{u}D_t$$

and is therefore proportional to the square of the characteristic length scale L_d

$$L_d = (Q_A/\bar{u})^{0.5}$$

(that is a characteristic dimension of the reacting plume, depending on flow rate and local fluid velocity) and inversely proportional to the local turbulent diffusivity (which in turn increases with N). In the conditions investigated the two characteristic times are generally of the same order, and therefore both micro- and mesomixing are important, but the relevance of mesomixing reduces at high N, as the ratio of the meso- and micromixing time is approximately proportional to $N^{-0.6}$ [27]. Figure 9 shows that increasing the flow rate τ_d increases, causing higher local supersaturation values and thus smaller crystal sizes, but Fig. 10 points out that also the feed bore, and thus the velocity of the feed at the outlet (or better its ratio to the velocity of the surrounding, $\bar{u}$) can be important.

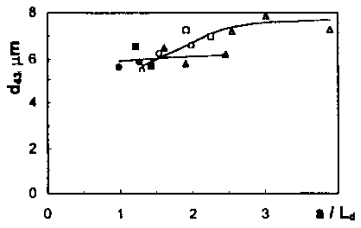

Fig. 11 Influence of mesomixing on crystal size at two rotation speeds: the ratio of feed tube diameter and the characteristic length scale for turbulent dispersion is given on the abscissa axis. Filled symbols, N=200 rpm; open symbols, N=500 rpm. Feed tube bore: ○ ●, 2 mm; □ ■, 3 mm; △ ▲, 4 mm. $S=10^4$

The feed pipe represents a local finite source if $a \approx L_d$ or $a > L_d$, and is much smaller than the characteristic dimension of the apparatus (i.e. the gap); in the cases investigated L_d ranged between 2.5 and 0.8 mm. Figure 11 points out the influence of the size of source and its relationship with the rotational speed: for intermediate values of N the crystal size increases initially with a/L_d, and then reaches an asymptotic value, while at low rotation speed practically no effect is observed.

Conclusions

The influence of the operating conditions in a Couette precipitator on the crystal properties have been investigated; the supersaturation ratio is the parameter that has the major effect both on the particle size and on the crystal morphology. The rotation speed has generally a relatively small effect; in certain conditions meso-mixing must be taken into account as the crystal size is influenced by feed tube diameter and feed velocity. The characteristic of the crystals are influenced by the experienced values of supersaturation, but the prediction of the influence of the operative parameters can be difficult: in fact, both the processes of nucleation and growth are determined by the local supersaturation, originated as a consequence of mixing, but an increase in the intensity of mixing can have an opposite effect, depending on the other operative conditions, because it can partially reduce the intensity of segregation of the unpremixed feeds, causing very high local values of supersaturation, or can allow a better homogeneity in the reaction volume, reducing the local supersaturation.

* * *

This work has been financially supported by the European Economic Community (Joule project JOU2-CT92-0127) and Italian Ministry of University (MURST 40% - Fluidodinamica Multifase).

Notation

a	feed tube inner diameter, m
A_P	particle surface, m^2
C_s	solid concentration, g l^{-1}
d	annular gap, m
d_{43}	volume weighed particle diameter, μm
d_p	particle diameter, μm
d_s	diameter of the sphere of equal volume, m
D_t	turbulent diffusivity, m^2 s^{-1}
H	height of inner cylinder, m
k_a	surface shape factor
k_v	volume shape factor
K_{ps}	solubility product of barium sulphate
L	characteristic size of the crystal, m
L_d	characteristic length scale for turbulent dispersion, m
N	rotation velocity of the inner cylinder, rpm
Q	flow rate of reactants, m^3 s^{-1}
r_1	inner cylinder radius, m
Re	rotational Reynolds number, $=r_1\Omega_1 d/\nu$
Re_z	axial Reynolds number, $=<w>d/\nu$

S initial supersaturation ratio, $=S=[Ba^{2+}][SO_4^{2-}]/K_{ps}$
S_{out} outlet supersaturation ratio
u local fluid velocity in the surrounding of the plume, m s^{-1}
V_p particle volume, m^3
$<w>$ average axial velocity, m s^{-1}

Greek letters

ν cinematic viscosity, m^2 s^{-1}
τ_d characteristic time for meso-mixing, s
Φ_v sphericity factor, def. in (3)
Ω_1 rotation speed of the inner cylinder, rad s^{-1}

References

1 N. S. Tavare, A. I. Ch. E. J., 32 (1986) 705.
2 J. Baldyga, Proc. 12th Symp. Industrial Crystallization (Z. H. Rojkowski, Ed.), Warsaw, Poland 1993, Vol. 1, paper I.2.1.
3 D. J. Gunn and M. S. Murthy, Chem. Eng. Sci., 27 (1972) 1293.
4 S. T. Liu, G. H. Nancollas and E. A. Gasiecki, J. Cryst. Growth, 33 (1976) 11.
5 J. Hostomsky, J. Rathousky and J. Skrivanek, Crystal Res. Technol., 16 (1981) 759.
6 M. S. Murthy, Chem. Eng. Sci., 49 (1994) 2389.
7 J. Baldyga, W. Podgórska and R. Pohorecki, Chem. Eng. Sci., 50 (1995) 1281.
8 N. Aoun, E. Plasari, R. David and J. Villermaux, Récents Prog. Génie Procédés, 9 (42, Génie des Procédés Complexes) (1995) 135.
9 N. Aoun, E. Plasari, R. David and J. Villermaux, Chem. Eng. Sci., 51 (1996) 2449.
10 K. Taguchi, J. Garside and N. S. Tavare, J. Cryst. Growth, 163 (1996) 318.
11 M. A. van Drunen, H. G. Merkus, G. M. van Rosmalen and B. Scarlet, Part. Syst. Charact., 13 (1996) 313.
12 G. Tosun, Proc. 6th Europ. Conf. Mixing (BHRA), Pavia, Italy 1988, 161.
13 R. Mohanty, S. Bhandarkar, B. Zuromski, R. Brown and J. Estrin, A. I. Ch. E. J., 34 (1988) 2063.
14 M. L. J. van Leeuwen, O. S. L. Druinsma and G. M. van Rosmalen, Chem. Eng. Sci., 51 (1996) 2595.
15 J. Baldyga and W. Orciuch, Trans. I. Chem. E., 75 A (1997) 160.
16 R. Kuboi, M. Harada, J. M. Winterbottom, A. J. S. Anderson and A. W. Nienow, Proc. 3rd World Congress Chemical Engineering, Tokio, Japan 1986, 1040.
17 J. Baldyga, R. Pohorecki, W. Podgórska and B. Marcant, Proc. 11th Symp. Industrial Crystallization (A. Mersmann, Ed.), Garmisch-Partenkirchen, RFG 1990, 175.
18 J. Chen, C. Zheng and G. Chen, Chem. Eng. Sci., 51 (1996) 1957.
19 R. Pohorecki and J. Baldyga, Proc. 5th Europ. Conf. Mixing (BHRA), Wurzburg, RFG 1985, 105.
20 R. Pohorecki and J. Baldyga, Chem. Eng. Sci., 43 (1988) 1949.
21 D. E. Fitchett and J. M. Tarbell, A. I. Ch. E. J., 36 (1990) 511.
22 W.-S. Kim and J. M. Tarbell, Chem. Eng. Commun., 146 (1996) 33.
23 D. Marchisio, A. A. Barresi and G. Baldi, Proc. 6th Int. Conf. Multiphase Flow in Industrial Plants, Milano, Italy 1998, 335.
24 B. Bernard-Michel, J. P. Testa, M. N. Pons and H. Vivier, Récents Prog. Génie Procédés 11 (51 Mixing 97) (1997) 365.
25 D. D. Archibald, B. P. Gaber, J. D. Hopwood, S. Mann and T. Boland, J. Crystal Growth, 172 (1997) 231.
26 H. Espig and H. Neels, Krist. Tech. 2 (1967) 401.
27 A. A. Barresi, D. Marchisio and G. Baldi, Chem. Eng. Sci., 54 (1999) 2339.